

1

**HY11491**

2

## **Uplift Pressures Below Spillway Chute Slabs at Unvented Open Offset**

3

### **Joints**

4

Tony L. Wahl, Member, P.E.<sup>1</sup>; K. Warren Frizell<sup>2</sup>;

5

and Henry T. Falvey, Life Member, Dr.Ing., Hon. D.WRE<sup>3</sup>

6

7

## **Abstract**

8 The catastrophic failure of the spillway chute at Oroville Dam in February 2017 raised concerns  
9 throughout the water resources industry regarding design, construction and maintenance  
10 practices for concrete spillway chutes, especially joints and cracks that could allow penetration  
11 of high pressure water into a chute foundation. The independent forensic team investigation  
12 found that hydraulic jacking was the most likely cause of the initial chute slab failure,  
13 highlighting a need for better analysis of the hydraulic jacking potential of existing spillways and  
14 more resilient designs for spillways that operate under high-velocity flow conditions. This paper  
15 reviews the Oroville Dam event and findings and previous laboratory testing performed to

<sup>1</sup> Technical Specialist, Bureau of Reclamation, Hydraulic Investigations and Laboratory Services, Denver, CO 80225-0007.

<sup>2</sup> Retired; formerly, Hydraulic Engineer, Bureau of Reclamation, Hydraulic Investigations and Laboratory Services, Denver, CO 80225-0007.

<sup>3</sup> Consultant, Henry T. Falvey & Associates, 11624 Blackfoot Rd., Conifer, CO 80433.

16 evaluate uplift pressures and flow transmitted through spillway joints. A reanalysis of previous  
17 studies was used to develop relations between chute velocity, joint geometry, and uplift pressure  
18 transmitted into a joint. Uplift pressure head in these relations is expressed in a dimensionless  
19 manner, either as a percentage of the velocity head in the boundary layer at the mid-height of the  
20 offset into the flow, or as a percentage of the channel-average velocity head. The first approach  
21 is potentially more useful for prototype applications, but the second method provides the best fit  
22 to the available experimental data. Additional research is still needed to quantify rates of flow  
23 through open joints, confirm relations between uplift pressure and boundary layer velocities, and  
24 evaluate the effects of aerated flow.

## 25 **Introduction**

26 The February 2017 failure of the spillway chute at Oroville Dam, owned and operated by the  
27 California Department of Water Resources (DWR), raises significant concerns about aging  
28 spillway structures. As dams and spillways age, concrete surfaces and masses slowly deteriorate,  
29 slabs may shift due to foundation settlement or frost heave, reinforcement bars and anchors may  
30 corrode and lose strength, and auxiliary components such as under-slab drain systems can be  
31 compromised by sediment deposition, scour, and intrusion of tree roots. Once concrete surfaces  
32 suffer initial deterioration, other problems become more likely, including cavitation damage,  
33 increased uplift forces at joints, and acceleration of deterioration rates due to freeze-thaw action.

34 One of the most likely locations for problems to occur in a concrete spillway chute is at or near  
35 the joints. Common types of joints include construction joints, control joints, expansion joints,  
36 and contraction joints. Joints typically deteriorate faster than slabs, and joints offer opportunities

37 for surface offsets and entry of pressurized flow into foundation areas, key elements for  
38 cavitation and hydraulic jacking failure modes. Even if uplift pressures are not large enough to  
39 cause immediate slab movement, the flows that enter the foundation through open joints can  
40 cause erosion and the development of voids beneath slabs that may ultimately lead to slab  
41 movement, offsetting of joints, and uplift. Despite these problems, joints are a practical  
42 necessity since spillways are large structures that typically must be constructed in a specific  
43 sequence and in multiple phases over several months or years. Joints placed at regular intervals  
44 enable staged construction, permit thermal contraction and expansion, and help to control cracks  
45 in the finished product. The geometry and construction details of joints vary, which affects their  
46 vulnerability to uplift and seepage flow. Although modern design standards for spillway joints  
47 (e.g., Bureau of Reclamation 2014) include details meant to prevent the development of offsets  
48 and gaps (e.g., keys and structural reinforcement) and limit flow through joints (waterstops),  
49 older spillways like Oroville lack some or all of these features or have other deficiencies (e.g.,  
50 poorly prepared foundations, inadequate or deteriorated drainage systems, etc.) that make them  
51 vulnerable to uplift failures.

52 Hydraulic jacking occurs when the forces acting to lift a spillway slab exceed the forces resisting  
53 upward movement. Resisting forces include the weight of the slab itself, the capacity of  
54 foundation anchors, and the pressure applied to the top of the slab by water flowing in the chute.  
55 Uplift can be created through a combination of increased pressure below the slab and reduced  
56 pressure above the slab (i.e., lift). High pressures can be generated below a slab when high-  
57 velocity flow stagnates against an offset into the flow at a joint that is open to the foundation.  
58 Offsets can occur due to settlement of an upstream slab or lifting or tilting of the edge of a  
59 downstream slab, or with no slab movement when the concrete surface is spalled upstream from

60 a joint. Slab movements that lead to offsets may occur due to drying or wetting of soil  
61 foundations, frost heave, or as a result of internal erosion of foundation soils when flow through  
62 open joints is not captured or retained within a drainage system. When internal erosion leads to  
63 the development of large voids beneath a slab, this may enable high pressures generated at a joint  
64 to more readily act over a large area beneath the slab.

65 Lift on the top surface of a slab can occur due to gradual curvature of the spillway surface away  
66 from the flow, or abrupt separations of flow from the spillway surface. Steps up or down caused  
67 by misalignment of joints are both capable of generating localized low pressure zones. Dong et  
68 al. (2010) studied cavitation at offsets into the flow and measured negative pressures  
69 approaching the vapor pressure of water in the separation zone downstream from 2- and 5-mm-  
70 high offsets, but pressure recovery was also observed to begin within 75 to 100 mm downstream.  
71 Vapor pressure establishes the minimum possible pressure on the upper surface of a spillway  
72 slab, limiting the contribution of flow separation to uplift head to about 10 m (33 ft), but  
73 stagnation pressure heads associated with high-velocity flow can be much larger. For example,  
74 the stagnation pressure associated with a velocity of 30 m/s (98 ft/s) is about 46 m (151 ft). For  
75 this reason, most analyses of uplift forces have focused on the pressure increase beneath the slab.  
76 In previous experimental work to be discussed later in this paper, the reported uplift is the net  
77 difference between the increased pressure below the slab and the pressure above the slab  
78 associated with a relatively shallow flow depth.

79 Additional factors that may be important in spillway slab uplift are air entrained in the flow  
80 above the slab and its effect on pressures generated within the joints, and the role of fluctuating  
81 pressures in combination with steady uplift. These two factors may also be linked to some

82 degree, as Bollaert and Schleiss (2003a, 2003b) have shown that air is an important factor in  
83 creating a resonance effect that magnifies pressure fluctuations within closed end fissures in  
84 fractured rock masses.

85 Hepler and Johnson (1988) and Trojanowski (2004) documented hydraulic jacking failures in  
86 Bureau of Reclamation spillways at Dickinson Dam (North Dakota) in 1954 and at Big Sandy  
87 Dam (Wyoming) in 1983. At Dickinson Dam there was a lack of defensive design features such  
88 as foundation grouting, anchor bars, and waterstops, and the underdrain system was  
89 compromised by subfreezing temperatures. In addition, there were several possible mechanisms  
90 that could have led to joints with offsets and openings that permitted pressurized flow to enter  
91 the foundation. Unfiltered gravel zones around the underdrain system were also implicated as a  
92 factor in internal erosion that led to the development of voids beneath the slabs. At Big Sandy  
93 Dam, freezing temperatures over many years caused deterioration of the spillway concrete,  
94 damage to the underdrain system, and slab movement that produced open and offset joints.

95 Uplift pressures at the time of failure were large enough to pull the foundation rock anchors out  
96 of the soft sandstone foundation (1.2-m [4-ft] long, 25-mm [1-inch] diameter bars on 1.5-m [5-ft]  
97 centers, with a design capacity of 44 kN [10 kips] each). It was speculated that the anchors may  
98 have been only 50 percent effective due to deterioration of the grout-foundation contact and  
99 could have been failed by an uplift pressure head greater than 49 percent of the mean velocity  
100 head, which was a feasible failure scenario (Trojanowski 2004). Considering these failures and  
101 experiences from other spillways exhibiting various types of distress, Trojanowski (2008)  
102 discussed the evaluation of potential failure modes of spillways, including factors related to  
103 hydraulic jacking.

# 104 **The Oroville Dam Spillway Failure**

105 The description of the Oroville Dam spillway chute failure incident given in this section is  
106 summarized from the report of the Oroville Dam Independent Forensic Team (IFT 2018).

107 Oroville Dam is an embankment dam located on the Feather River in northern California—the  
108 tallest dam in the United States at 235 m (770 ft). The dam is owned and operated by DWR,  
109 which was responsible for design and construction, completed in 1968. The dam is one  
110 component of the Oroville-Thermalito Complex, which includes several hydroelectric  
111 powerplants, canals, and diversion and fish barrier dams. The complex is a major feature of the  
112 California State Water Project, the largest state-owned water storage and delivery system in the  
113 United States. On February 7, 2017 the service spillway chute lining failed, leading to an  
114 emergency that lasted for several weeks while the spillway was required to continue operating.

115 At the time of the failure Oroville Dam was equipped with two spillways. The gated spillway,  
116 described as the service spillway or Flood Control Outlet (FCO), was controlled by eight large  
117 top-seal radial gates and discharged into a concrete chute that was 54.5 m (178.67 ft) wide and  
118 914 m (3000 ft) long. The emergency spillway, which had never operated, was a 518-m (1700-  
119 ft)-long uncontrolled overflow weir discharging into an unimproved steep natural drainage  
120 leading back to the Feather River. The service spillway chute was originally designed for a  
121 maximum flow rate of 7080 m<sup>3</sup>/s (250,000 ft<sup>3</sup>/s). The historical maximum instantaneous  
122 discharge was 4530 m<sup>3</sup>/s (160,000 ft<sup>3</sup>/s) in 1997, about 64% of the design discharge (IFT 2018).  
123 The spillway had operated infrequently in its 49 year history, with about 4 days of operation  
124 above 2830 m<sup>3</sup>/s (100,000 ft<sup>3</sup>/s), 40 days above 2120 m<sup>3</sup>/s (60,000 ft<sup>3</sup>/s), and 300 days above

125 1060 m<sup>3</sup>/s (30,000 ft<sup>3</sup>/s). Soon after construction was completed, cracking of the spillway slab  
126 occurred over embedded drain pipes, which were arranged in a herringbone pattern down the  
127 length of the spillway. As result, there was a long history of periodic repairs made to maintain  
128 the service spillway chute slab.

129 Due to heavy snow and rain in northern California in the winter of 2016-2017, the service  
130 spillway operated for about 5 days in mid-January 2017 at flow rates up to about 283 m<sup>3</sup>/s  
131 (10,000 ft<sup>3</sup>/s), the first significant flows since 2011. The spillway was shut down around January  
132 20 and then restarted around February 1. Discharges were gradually increased during early  
133 February. At about 10:10 a.m. on the morning of February 7, while the discharge was being  
134 increased from 1200 to 1490 m<sup>3</sup>/s (42,500 ft<sup>3</sup>/s to 52,500 ft<sup>3</sup>/s), DWR personnel working near the  
135 left side of the service spillway chute heard a loud sound they compared to an explosion. They  
136 subsequently observed spray and significantly disturbed flow conditions in the spillway chute  
137 near station 1020 m (33+50 ft), about 640 m (2100 ft) downstream from the spillway radial  
138 gates. The spillway continued to operate for about one hour, and then from about 11:25 a.m. to  
139 12:25 p.m. the spillway gates were closed, revealing the damage shown in Figure 1.

140 Due to forecasted large inflows, a continued need for spillway operations was anticipated.  
141 Following initial damage assessments and release of some closely monitored test flows, the  
142 spillway was placed back into service from Feb. 8-10 at discharges up to 1840 m<sup>3</sup>/s (65,000  
143 ft<sup>3</sup>/s), with erosion and damage to the chute structure continuing. Unfortunately, these releases  
144 were not enough to keep up with inflow to the reservoir. Early on February 11 the reservoir  
145 level exceeded elev. 274.62 m (901 ft) and the emergency spillway began to flow for the first  
146 time in its history. The reservoir level eventually reached elev. 275.11 m (902.59 ft) at about

147 3:00 a.m. on February 12, with a peak flow of about 354 m<sup>3</sup>/s (12,500 ft<sup>3</sup>/s) over the emergency  
148 spillway crest. There was extensive erosion and headcutting in the natural channel below the  
149 emergency spillway crest, and headcuts advancing upstream toward the spillway crest threatened  
150 its stability. At 3:35 p.m. on February 12 the service spillway gate openings were increased to  
151 draw the reservoir down and reduce flows over the emergency spillway crest. At 3:44 pm on  
152 February 12, an evacuation order was issued for about 188,000 downstream residents due to the  
153 rapidly progressing erosion in the emergency spillway discharge channel. The service spillway  
154 flows reached 2830 m<sup>3</sup>/s (100,000 ft<sup>3</sup>/s) by about 7:00 p.m. on February 12 and were maintained  
155 there for about 3.5 days through 8:00 a.m. on February 16. During this period the reservoir  
156 levels dropped significantly and the situation stabilized. Service spillway flows were gradually  
157 reduced over subsequent days until the spillway was shut down again on February 27. After new  
158 inspections, the service spillway was placed back into operation in early March and operations  
159 continued until it was shut down for the season on May 19. The damage to the spillway at the  
160 end of the operating season is shown in Figure 2.

## 161 **Forensic Investigation**

162 A six-member Independent Forensic Team (IFT) (including the third author) was formed after  
163 the Oroville Dam spillway slab failure, with the following charge:

164 *“To complete a thorough review of available information to develop findings and opinions*  
165 *on the chain of conditions, actions, and inactions that caused the damage to the service*  
166 *spillway and emergency spillway, and why opportunities for intervention in the chain of*  
167 *conditions, actions, or inactions may not have been realized.*

168 Their report issued in January 2018 provides the IFT's opinion on the physics of the failure  
169 process and the most likely failure modes. The report also identifies physical factors and  
170 features of the design that contributed to the failure and identifies organizational and human  
171 factors that contributed to the failure and affected the response to the emergency.

172 The IFT concluded that the spillway chute failure most likely was initiated by uplift and removal  
173 (hydraulic jacking) of a section of the chute slab near Sta. 1020 m (33+50 ft), just downstream  
174 from the end of the vertical curve in the chute that transitions from a 5.67% slope to a 24.5%  
175 slope. High-velocity flow then rapidly eroded moderately to highly weathered rock and soil-like  
176 foundation materials beneath adjacent slabs. The initial uplift failure was believed to have affected  
177 only part of one of the 12.2- by 15.2-m (40- by 50-ft) chute slab panels, and could have removed  
178 something as small as a localized repair patch or a spall above a drain, or as large as a 6-m (20-ft)  
179 section located between cracks that existed above the herringbone drains partially embedded in the  
180 bottom of the slab. Once the initial portion of the slab failed, it probably triggered a rapid chain of  
181 subsequent events, leading to additional slab section failures (IFT 2018).

182 The IFT report discussed the possibility of an initial failure due to sagging or settling of a slab into a  
183 void beneath the slab. The team could not absolutely rule out this possibility, but found it less likely  
184 than an uplift failure for several reasons, including the suddenness of the failure, eyewitness reports  
185 of explosion-like sounds, and a lack of any evidence of sagging in photos taken of the spillway after  
186 the operations in early January 2017. The team also allowed for the possibility that localized  
187 settlement upstream from a joint or crack could have created an offset into the flow that led to  
188 injection of high pressure water beneath the slab downstream from that location.

189 **Contributing Factors**

190 Several physical factors were cited by the IFT that contributed to the initial failure and  
191 subsequent damage to the spillway chute. Although the team was confident that the initial  
192 failure occurred due to uplift created by high-velocity flow being injected through a feature of  
193 some kind in the chute slab surface, they could not pinpoint the specific type or exact location of  
194 the feature. Possibilities they listed included: open joints, unsealed cracks over lateral drainage  
195 pipes (the herringbone drains), spalled concrete at either a joint or drain location in a new or  
196 previously repaired area, or some combination of multiple features. The IFT made calculations  
197 of potential discharges through cracks and joints and believed that the flows could have far  
198 exceeded the localized capacity of the drain system, causing flow to back up in the drains and  
199 increase uplift forces.

200 Several contributing factors were specifically listed by the IFT as possible explanations for why  
201 the spillway chute failed in 2017 at a discharge of about 1490 m<sup>3</sup>/s (52,500 ft<sup>3</sup>/s), but had not  
202 failed in earlier high-flow events, such as a release of more than 1980 m<sup>3</sup>/s (70,000 ft<sup>3</sup>/s) in 2006  
203 and the maximum discharge of 4530 m<sup>3</sup>/s (160,000 ft<sup>3</sup>/s) in 1997. All of these contributing  
204 factors are related to slow changes in the condition of the spillway materials or foundation over  
205 time.

- 206 • New chute slab damage and/or deterioration of previous slab repairs,
- 207 • Expansion of relatively shallow void(s) under the slab, through erosion or shrinkage of  
208 clay soils,
- 209 • Corrosion of steel reinforcing bars or dowels across the concrete cracks or joints, and
- 210 • Reduction in anchor capacity

## 211 **Hydraulic Analyses**

212 Appendix B of the IFT's report provided detailed analysis and discussion of hydraulic  
213 phenomena that were considered by the team in connection with their efforts to identify the  
214 initiating cause of failure and contributing factors.

### 215 ***Stagnation and Uplift Pressures***

216 To evaluate the potential uplift pressures that could act on a spillway slab, the IFT report  
217 described an approach to estimating the stagnation pressure that could occur at a vertical offset  
218 into the flow. When flow strikes the face of such an offset, flow is deflected downward into the  
219 joint and up and over the offset. At the dividing line between these flows, the flow stagnates  
220 against the face of the offset and the kinetic energy of the flow is converted into potential energy  
221 in the form of pressure head—the *stagnation pressure*. With an opening in the joint, all or a  
222 portion of the stagnation pressure can be transmitted through the joint, creating uplift beneath the  
223 slab. The stagnation pressure can also drive flow into the joint, and this flow must be carried  
224 away by the drainage system beneath the slab to avoid a buildup of pressure.

225 In a prototype spillway with a long chute, a velocity profile develops in the chute with low  
226 velocities near the bed and high velocities near the water surface. The greatest variation of  
227 velocities occurs very near the bed in the boundary layer. At a significant distance down the  
228 chute, the thickness of the boundary layer could be enough for offsets at spillway joints to be  
229 contained entirely within the boundary layer. In this case, flow offsets would be exposed to  
230 velocities that are lower than the average velocity within the whole channel. Referring to studies  
231 of flow over open offset joints by Frizell (2007) that utilized Particle Image Velocimetry (PIV)  
232 to map velocity fields approaching a joint, the IFT report suggested that the streamline of the

233 flow stagnating against the face of an offset into the flow tended to be located at about half of the  
234 offset height. With the failure taking place about 640 m (2100 ft) downstream from the control  
235 gates, the boundary layer was estimated to have a thickness of about 1 m (3.3 ft), with a well-  
236 developed velocity profile in the channel. To estimate the velocity at various heights above the  
237 channel floor that might correspond to the mid-height of offsets of different sizes, the IFT used  
238 an equation provided by Rouse (1945, p. 199, Eq. 157) to describe the velocity profile versus  
239 depth in an open channel flow:

$$240 \quad \frac{v_y - V}{V\sqrt{f}} = 2 \log_{10} \frac{y}{y_0} + 0.88 \quad (1)$$

241 where  $v_y$  = velocity at distance  $y$  above the boundary

242  $f$  = Darcy-Weisbach friction factor

243  $y$  = distance from the boundary

244  $y_0$  = total flow depth

245  $V$  = mean flow velocity

246 It is important to note that  $y_0$  is the total flow depth and that Eq. 1 computes an estimate of the  
247 entire velocity profile from the boundary to the free surface, not just the velocity within the  
248 boundary layer near the bed. (The IFT report incorrectly identified  $y_0$  as the depth where the  
249 velocity is zero.) This equation is sensitive to the surface roughness through the friction factor,  $f$ ,  
250 so rougher surfaces will have a more pronounced velocity profile with lower velocities near the  
251 channel bed. Once  $v_y$  is estimated, the associated stagnation pressure is

$$252 \quad \frac{P_s}{\gamma} = \frac{v_y^2}{2g} \quad (2)$$

253

254 where  $P_s$  = stagnation pressure

255  $\gamma$  = unit weight of water

256  $v_y$  = approach velocity of the stagnated flow

257  $g$  = acceleration due to gravity

258 Table 1 shows stagnation pressures estimated at 50% of the offset height for two flow rates and  
259 three joint offset heights. The two flow rates bracket the conditions at the time of the initial  
260 Oroville failure, and the flow depths and velocities at the station of the failure are determined  
261 from water surface profile calculations (Falvey 1990; Wahl et al. 2019), assuming a surface  
262 roughness of 0.3 mm (0.001 ft). This table is similar to Table 2 in Appendix B of the IFT report,  
263 but corrects three problems that affected that table: 1) velocities were calculated at the tip of the  
264 offset, even though the text of the IFT report said they were calculated at the mid-height; 2)  
265 stagnation pressure head values were actually velocities that had not yet been converted to  
266 pressure head; and 3) incorrect friction factors were used that were much too large. In the  
267 present Table 1, friction factors were determined with the Colebrook-White equation as an  
268 integral part of the water surface profile calculations. In this particular example, the combined  
269 corrections for these three problems largely offset one another, so the numerical values of  
270 stagnation pressure head in Table 1 are not dramatically different from those given in the IFT  
271 report.

272 The stagnation pressures shown in Table 1 can become the source for generating uplift pressure  
273 beneath a slab, but the IFT report emphasized that there is uncertainty regarding the extent over  
274 which the uplift force would act. The type of drain system beneath the joint or the porosity and

275 permeability of soils beneath the joint would affect the distribution and extent of uplift pressures.  
276 The IFT report did not estimate a probable pressure distribution or total uplift force on a whole  
277 slab or portion of a slab, but used the analysis only to show the magnitude of uplift pressures that  
278 could have been generated and the trends for increasing uplift pressure with increasing discharge.  
279 The stagnation pressure head increases 22% when the flow rate increases 80% from 850 to 1530  
280  $\text{m}^3/\text{s}$  (30,000  $\text{ft}^3/\text{s}$  to 54,000  $\text{ft}^3/\text{s}$ ). Note that the estimated stagnation pressures are small  
281 fractions (30% to 50%) of the total velocity head of the mean flow, which illustrates the  
282 significant effect of basing the stagnation pressure estimates on the velocity near the surface,  
283 rather than on the mean channel velocity. This analysis is sensitive to the assumed hydraulic  
284 roughness of the flow surface. With increased roughness the calculated stagnation pressures  
285 drop significantly and there is greater sensitivity to the offset height.

286 The analytical approach taken by the IFT depended on some significant assumptions. For a  
287 given joint offset height, the uplift pressure is estimated by assuming that stagnation of the  
288 velocity occurs at 50% of the offset height, and that 100% of this stagnation pressure is  
289 transmitted through the joint. Each of these assumptions should be verified with either lab or  
290 field testing. In addition, to apply this analysis to the practical problem of determining the net  
291 uplift force, the drainage system and/or underlying foundation must be analyzed to determine  
292 how drainage will dissipate the uplift pressure. Once the resulting uplift forces are estimated, the

293 design of the slab and its anchorage can be evaluated to determine if the slab can withstand the  
294 applied loads.

### 295 ***Flow through Joints or Cracks***

296 The IFT report analyzed the potential for seepage or leakage flow through open spillway joints  
297 or cracks. The analysis used the energy equation applied to the slot behaving as a pressurized  
298 conduit experiencing turbulent flow. The analysis considered only joints and cracks that were  
299 flush, with no offset into or away from the flow. The driving force for flow through the joint  
300 was only the hydrostatic pressure associated with the spillway flow depth, not any stagnation  
301 pressure. No quantitative estimates were made of the density of cracking in the slab or the  
302 prevalence of open joints, but the IFT found that the drainage system beneath the Oroville Dam  
303 spillway chute would have been unable to convey the volume of flow that might have come from  
304 the widespread open joints or cracks.

305 The analysis performed by the IFT did not consider the increased flow through a joint that could  
306 occur due to stagnation pressure developing against the entrance to an offset joint. Laboratory  
307 testing has not yet provided reliable information that can be used for this purpose.

## 308 **Previous Research**

309 Despite the historical cases of spillway chute slab failure by hydraulic jacking, efforts to quantify  
310 the uplift pressures generated by high-velocity flows over offset and open spillway joints have  
311 been very limited. Most studies of uplift have focused on slabs and joints in stilling basins and  
312 plunge pools, where fluctuating pressures generated by hydraulic jumps and impinging jets are  
313 the driving mechanism (Toso and Bowers 1988; Fiorotto and Rinaldo 1992a, 1992b; Bellin and

314 Fiorotto 1995; Fiorotto and Salandin 2000; Melo et al. 2006; Liu and Li 2007; Mahzari and  
315 Schleiss 2010; González-Betancourt and Posada-García 2016). Bowers and Toso (1988)  
316 describe a model study intended to study this mechanism in the failure of one specific spillway  
317 stilling basin. Fiorotto and Caroni (2014) and Barjastehmaleki et al. (2016a, 2016b) considered  
318 how the high pressures generated at stilling basin slab joints propagate beneath the slab and  
319 dissipate with increasing distance from the joint.

320 High pressures generated in the joints and cracks of rock masses have also been studied  
321 extensively as a driving mechanism for scour in rocky plunge pools and unlined rock channels  
322 (Bollaert and Schleiss 2005; Pells 2016), but not with a focus on joints with the regularity or  
323 extent of those found in concrete spillway linings. Most of this work has been directed toward  
324 the prediction of removal of individual rock blocks or the breakup of large rock masses into  
325 smaller units due to intense pressure fluctuations on rock surfaces or within joints. Key features  
326 of the flows driving these processes are impingement of jets at angles ranging from normal to  
327 acute, aeration and disintegration of jets both above and below the water level of the pool, and  
328 sizable pressure fluctuations applied to slab surfaces and joints. These characteristics stand in  
329 sharp contrast to gradually varied flows that are essentially parallel to relatively smooth spillway  
330 chutes. The flume study by Pells (2016) produced measurements of pressure generated within  
331 the joints surrounding an idealized rock block projecting into a high-velocity open-channel flow  
332 similar to that in a spillway chute, but included many three-dimensional effects that would be  
333 absent or much different for flow over a typical chute slab joint.

334 To the authors' knowledge, the only studies of uplift pressure due to unidirectional high-velocity  
335 flow over offset spillway joints are those of Johnson (1976) and Frizell (2007), both conducted in

336 the Hydraulics Laboratory of the Bureau of Reclamation. Those two studies will be reviewed  
337 here and the data further analyzed with a view toward application to situations like the event at  
338 Oroville Dam.

## 339 **Open-Channel Tests**

340 Johnson (1976) studied uplift pressures beneath spillway chute slabs using a 152-mm (6-inch)  
341 wide by 2.44-m (8-ft) long open channel flume that contained an open joint with a vertical offset  
342 into the flow located 0.91 m (3 ft) from the downstream end. The width of the joint opening  
343 (gap) was set to values of 3.2, 6.4, 12.7, and 38.1 mm ( $\frac{1}{8}$ ,  $\frac{1}{4}$ ,  $\frac{1}{2}$ , and  $1\frac{1}{2}$  inches) and the size of  
344 the vertical offset was set to 3.2, 6.4, 19.1, and 38.1 mm ( $\frac{1}{8}$ ,  $\frac{1}{4}$ ,  $\frac{3}{4}$ , and  $1\frac{1}{2}$  inches). In photos,  
345 the flume appears to be level, but the exact slope is undocumented. Flow was provided through  
346 an adjustable vertical slide gate that allowed the flow velocity at the offset to be varied from 2.29  
347 to 4.57 m/s (7.5 to 15 ft/s), as measured by a Pitot tube (presumably positioned upstream from  
348 the offset joint). The open joint allowed water to enter a chamber beneath the flume that was  
349 tightly sealed. Pressures in this chamber were measured using a dynamic pressure transducer  
350 whose output was recorded on a strip-chart. The joints studied were all oriented normal to the  
351 bed of the flume and extended perpendicular to the flow direction across the full width of the  
352 flume.

353 Average pressure values and a value that exceeded 95% of the instantaneous dynamic pressures  
354 were both determined from the strip-chart records. The latter was arbitrarily selected as a value  
355 representative of maximum uplift pressures at a spillway slab. Net uplift pressure heads were  
356 reported as the difference between the high pressure in the chamber and the average depth of  
357 flow measured over the joint, but separate pressure and depth measurements were not reported.

358 Uplift pressure heads were presented as dimensionless percentages of the computed velocity  
359 head corresponding to the average flow velocity in the channel for each test, but the data were  
360 not analyzed using any dimensionless measure of the offset heights and gap widths. Also,  
361 although the discussion suggested that uplift pressures should be related to the conditions in the  
362 boundary layer and that trends in observed uplift in the experiments were consistent with this  
363 idea, no attempt was made to quantitatively relate the uplift pressures to boundary layer  
364 velocities instead of the channel-average velocity. Boundary layer characteristics were not  
365 measured during the experiments, nor were any attempts made to analytically estimate the  
366 boundary layer conditions of the tests.

367 Notable trends observed in the data were:

- 368 • Uplift pressures increased with smaller gap widths. This was attributed to larger gaps  
369 allowing larger or stronger flow circulation cells to develop within the gap, dissipating  
370 some of the flow energy and reducing the uplift pressure transmitted through the gap.  
371 Another explanation is that a larger portion of the gap width was exposed to pressures  
372 below the stagnation pressure, since true stagnation of the flow only occurs at the face of  
373 the offset.
- 374 • Uplift pressures increased for larger vertical offsets, most rapidly when vertical offsets  
375 were small. At large vertical offset heights, the uplift pressure tended to approach a  
376 constant percentage of the velocity head.
- 377 • For higher velocities, the uplift pressures tended to be a slightly smaller percentage of the  
378 channel-average velocity head.

379 Specific flow depths, discharges, and channel slope data for each test were not reported.  
380 However, the short distance from the entrance of the flume to the joint location suggests that the  
381 boundary layer in these tests was relatively thin.

382 Figure 3 shows the Johnson (1976) measurements of average uplift pressures in a format that is  
383 condensed, but similar to the way they were first presented by Johnson. Uplift pressures are  
384 made dimensionless by expressing them as a percentage of the channel-average velocity head.  
385 Johnson originally showed data for each gap width on a separate plot, with individual hand-draw  
386 curves passing through the data points collected at each velocity setting. In this condensed  
387 presentation Figure 3 shows power curves through the data for each gap width to illustrate  
388 general trends in the data. Johnson's observations highlighted previously are apparent,  
389 especially the significant increase in uplift pressure as the width of the joint gap was reduced.  
390 Although the data are not included here, trends in the 95-percent maximum uplift pressure data  
391 were similar, with the 95-percent maximum uplift typically being about 1.15 to 1.40 times the  
392 average uplift.

## 393 **Water Tunnel Tests**

394 The second significant study of the uplift pressure phenomenon was conducted at Reclamation  
395 by the second author (Frizell 2007) using a high-head pump to deliver high-velocity flow to a  
396 pressurized water tunnel containing an idealized spillway joint that could be adjusted to create  
397 offset heights of 3.2, 6.4, 12.7, and 19.1 mm ( $\frac{1}{8}$ ,  $\frac{1}{4}$ ,  $\frac{1}{2}$ , and  $\frac{3}{4}$  inches) and gap widths of 3.2, 6.4,  
398 and 12.7 mm ( $\frac{1}{8}$ ,  $\frac{1}{4}$ , and  $\frac{1}{2}$  inch). The layout of the test facility is shown in Figure 4, with the  
399 test section located downstream from a tee on the pump discharge line. The tests could be  
400 conducted with flow velocities of about 5.2 to 14.6 m/s (17 to 48 ft/s) in the 102-mm wide by

401 102-mm tall (4-inch by 4-inch) section approaching the offset (Figure 5). The exit height of the  
402 test section was reduced from the nominal 102-mm (4-inch) dimension by the height of the  
403 offset. In addition to the tests with rectangular sharp-edged joint geometries, tests were also  
404 performed on joint openings with 3.2-mm by 3.2-mm ( $\frac{1}{8}$ -inch by  $\frac{1}{8}$ -inch)  $45^\circ$  chamfered edges  
405 and 3.2-mm ( $\frac{1}{8}$ -inch) radius edges. Tests were conducted in a sealed configuration, where no  
406 flow could exit the chamber beneath the spillway joint, and a vented condition in which flow  
407 could exit through a valve. The size of the exit valve was not reported, but its flow capacity was  
408 not enough to keep the chamber fully vented. As a result, back pressure existed below the  
409 spillway joint in the vented tests, but it was not directly measured. Uplift pressures were  
410 measured with a differential pressure transducer connected to taps above and below the movable  
411 downstream block (Figure 6). Particle Image Velocimetry (PIV) was also used to map velocity  
412 fields above and within the joint for a small subset of the tests (chamfer-edged joints with 3-mm  
413 [ $\frac{1}{8}$ -inch] and 13-mm [ $\frac{1}{2}$ -inch] gap widths and 13-mm [ $\frac{1}{2}$ -inch] offset heights). Finally,  
414 accompanying computational fluid dynamics (CFD) models were configured and run using the  
415 FLOW-3D software package developed by Flow Science, Inc. CFD models were created to  
416 simulate both the test facility and a prototype spillway joint. The PIV measurements and CFD  
417 models were used primarily to visualize the flow field in the vicinity of the joints. There is  
418 potential for CFD studies to be used to study uplift pressures, but quantitative uplift pressure  
419 results were not provided in this study.

420 The collected uplift pressure data were originally presented by Frizell (2007) in plots showing  
421 the raw differential pressures versus the average velocity over the offset (at section 2 in Figure  
422 6). These plots verified that uplift pressure was proportional to the square of the velocity and  
423 that uplift pressures also increased with increasing offset height, but the data were not presented

424 in a dimensionless manner that would allow direct comparison to the Johnson (1976) results.  
425 The uplift pressures tended to decrease in most cases with increasing gap widths, similar to the  
426 observation by Johnson (1976). Frizell (2007) also observed that boundary layer effects could  
427 have a substantial impact in a prototype, but made no analysis of the boundary layer conditions  
428 that existed in the tests, presuming that the boundary layer was thin and that uplift pressures  
429 would be related to the mean velocities. The tests of chamfered-edged and radius-edged joint  
430 openings showed similar trends as the tests of sharp-edged openings, with a tendency for the  
431 chamfered- and radius-edged openings to behave like sharp-edged openings of a slightly larger  
432 dimension.

433 In the water tunnel experiments Frizell (2007) employed a differential pressure transducer  
434 connected to piezometer taps below and above the downstream slab and reported that differential  
435 pressure as the uplift pressure. However, the use of the water tunnel causes three effects that  
436 distort this measure of uplift pressure. First, there is an increase in velocity head from the  
437 section upstream from the joint (section 1 in Figure 6) to the section downstream from the offset  
438 (section 2) due to the reduced height of the tunnel caused by the vertical offset. The lower  
439 velocity head at section 1 will be accompanied by a higher pressure head than that at section 2.  
440 The pressure in the sealed chamber beneath the slot should be expected to reflect this larger  
441 pressure head. Second, there is a loss of head at the offset due to the minor loss created by the  
442 contraction itself. This also causes an increase in pressure at section 1. Finally, there is also a  
443 friction loss in the water tunnel that creates an additional pressure difference between the two  
444 sections. Each of these three pressure difference contributors must be subtracted from the  
445 measured pressure difference to determine the uplift caused by the stagnation of flow against the  
446 face of the vertical offset.

447 Similar head losses and flow changes occur in an open channel flow, but they affect the uplift  
448 pressure beneath the slab differently. In the supercritical flows tested by Johnson (1976), there  
449 was an increase in depth in the downstream direction as the flow passed over the offset and  
450 experienced contraction and friction losses. (In a subcritical flow, the depth would decrease in  
451 the downstream direction due to friction and contraction losses and the step-up in the channel  
452 bottom). However, there was no way for this depth increase to affect the flow upstream from the  
453 face of the offset or the uplift generated by the step, since pressure waves cannot travel upstream  
454 in supercritical flow. The conditions in the sealed chamber could only be influenced by the flow  
455 upstream from the offset. The increased downstream depth did have a small effect on the  
456 pressure above the downstream slab. Although Johnson explained that he subtracted out the  
457 flow depth when reporting the net uplift pressures, he did not definitely state whether he  
458 measured the flow depth upstream or downstream from the offset. It is presumed that the  
459 measurement was made downstream from the offset, since uplift of the downstream slab was of  
460 interest, but the difference in either case would be small (probably less than 25 mm = 1 inch).

461 In the water tunnel configuration the head losses and pressure changes associated with  
462 pressurized flow are substantial in comparison to the measured differential pressure heads.  
463 Unfortunately, there were no actual measurements of these head losses or the total head losses  
464 made during the tests. Therefore, estimates of each loss were calculated during the present  
465 review, and these were used to compute adjusted values of uplift pressure head that could be  
466 compared directly to the open channel data from Johnson (1976). The velocity head change was  
467 the most readily and accurately estimated, based on the cross section dimensions and offset  
468 height, and varied from about 14% to 50% of the measured differential pressure head. The  
469 contraction loss was estimated from equations for computing minor losses at abrupt concentric

470 pipe contractions (Roberson and Crowe 1985) and ranged from 3% to 14% of the measured  
471 differential pressure head. The friction loss estimates had significant uncertainty depending on  
472 the assumed values of surface roughness in the test section, but were smaller than the other two  
473 effects, ranging from about 2% to 6% of the measured differential pressure head. The combined  
474 effects of all three components ranged from 20% to 66% of the measured differential pressure  
475 head.

### 476 **Flow through Joints**

477 The Frizell (2007) study reported flow rates through the joints in a vented condition, but a review  
478 of the data and the analysis procedures now shows that the pressure measurements used to  
479 indirectly determine the discharges did not accurately reflect actual flow rates. Future tests of  
480 flow through open joints should use calibrated, direct flow measurement methods and include  
481 measurements of the back pressure beneath the open joint. Running tests in a fully vented  
482 condition (with a much larger outlet valve) would provide an indication of the maximum flow  
483 that can occur through a joint experiencing no back pressure from the underlying foundation or  
484 drainage system.

## 485 **Analysis**

486 The IFT (2018) approach to estimating uplift pressure head for the Oroville Dam spillway was to  
487 estimate the velocity profile in the channel, specifically the velocity occurring at a distance  
488 above the channel bed equal to half of the height of an offset into the flow. The uplift pressure  
489 was then equal to the velocity head at this point in the profile. The two experimental data sets  
490 from Johnson (1976) and Frizell (2007) offer an opportunity to test this concept, but since

491 velocity profiles were not measured in either study, the mid-height velocity must be estimated by  
492 analytical means.

493 In the Johnson (1976) open channel experiments it is reasonable to assume that the development  
494 of the boundary layer began at the slide gate that controlled the inflow, 1.52 m (5 ft) upstream  
495 from the simulated joint. For the Frizell (2007) water tunnel experiments, the boundary layer  
496 development can be assumed to begin at the upstream end of the square duct leading to the test  
497 section, 1.72 m (5.66 ft) upstream from the simulated joint. (The velocity was rapidly  
498 accelerating in the round-to-square transition leading to the square duct, almost tripling in a  
499 distance of 0.91 m [3 ft].) For both cases the velocity profile in the boundary layer can be  
500 estimated from (Roberson and Crowe 1985, Eq. 9-27):

501 
$$v_y = u_* \left( 5.75 \log_{10} \frac{yu_*}{\nu} + 5.56 \right) \quad (3)$$

502 with  $u_*$  being the shear velocity and  $\nu$  being the kinematic viscosity of the fluid. In the early  
503 phase of boundary layer growth, the value of  $u_*$  is a function of the distance from the point of  
504 boundary layer initiation and is given by a set of three equations (Roberson and Crowe 1985, pp.  
505 321-336, Eqs. 9-19 and 9-42):

506 
$$u_* = \sqrt{\frac{\tau_0}{\rho}} \quad (4)$$

507 
$$\tau_0 = \frac{0.058}{5} \frac{\rho V^2}{\sqrt{\text{Re}_x}} \quad (5)$$

508 
$$\text{Re}_x = \frac{Vx}{\nu} \quad (6)$$

509 where  $\rho$  is the fluid density and  $V$  is the mean channel velocity (the free-stream velocity outside  
510 of the boundary layer), and  $x$  is the distance from the start of boundary layer growth. This yields  
511 a straightforward way to calculate the boundary layer velocity profile as a function of the mean  
512 velocity of the flow. In addition, the thickness of the boundary layer at distance  $x$  can be  
513 estimated from (Roberson and Crowe 1985, Eq. 9-41):

514 
$$\delta = \frac{0.37x}{\sqrt[5]{\text{Re}_x}} \quad (7)$$

515 Applying Eq. 7 to the Johnson (1976) tests, the boundary layer thickness at the test location  
516 varied from about 24.4 to 27.9 mm (0.96 to 1.1 inches), decreasing with increasing velocity, so  
517 the 38.1-mm (1.5-inch) offsets would have extended into the free stream flow, but offsets of  
518 19.1 mm (0.75 inches) or less would have been fully contained in the boundary layer. For the  
519 Frizell (2007) tests, the boundary layer thickness varied from about 21.4 to 26.1 mm (0.84 to  
520 1.03 inches), which is larger than all of the tested offset heights.

521 Johnson (1976) analyzed the uplift pressure head as a dimensionless percentage of the mean-  
522 channel velocity head, but related it to dimensional offset heights and gap widths of the tested  
523 joints. Frizell (2007) plotted the dimensional uplift pressure head versus the mean flow velocity  
524 for different offset heights and gap widths. To generalize the results in a more useful way,  
525 Figure 7 presents both sets of data plotted using a fully dimensionless approach. This figure  
526 includes the data for all gap widths, offset heights, and velocities tested by Johnson (1976) and  
527 all of the sealed-cavity, sharp-edged joint tests conducted by Frizell (2007). The average uplift  
528 pressure heads are presented as percentages of the stagnation pressure computed for the  
529 estimated boundary layer velocity at the mid-height of the offset, computed using equations 3-6.  
530 The dimensionless uplift pressures are plotted as a function of the dimensionless ratio of gap

531 width to offset height, with the data subdivided by distinct values of offset height. This  
532 presentation collapses the data more effectively than Figure 3, indicating that uplift pressures  
533 approach 100% of the mid-height boundary layer velocity head as the ratio of gap width to offset  
534 height is reduced toward zero. The plots show clearly that there is a reduction in the developed  
535 uplift pressure for relatively wide gap width to offset height ratios, in contrast to the IFT (2018)  
536 assumption that the uplift pressure would be equal to the velocity head at mid-height of the  
537 offset, independent of the gap width dimension. The plots show that there was some dependence  
538 in the experiments on the dimensional offset height, with the data following somewhat higher  
539 curves for smaller offsets, especially the open channel data. In general, the water tunnel data  
540 exhibit slightly larger dimensionless uplift values at low gap to offset ratios and smaller values at  
541 high ratios. These differences could be due to several factors, including viscous (Reynolds) scale  
542 effects, uncertainties in the estimates of boundary layer velocity profiles, or uncertainties related  
543 to the uplift pressure adjustments applied to the water tunnel data. A curve fit to the combined  
544 data from both studies (Figure 8) produces Equation 8 with an  $R^2$  value of 0.68, which can be  
545 used to predict the uplift pressure head:

546 
$$\frac{H_u}{V_{bl}^2/(2g)} = e^{0.055-0.417\sqrt{\beta}} \quad (8)$$

547  $H_u$  is the uplift pressure head,  $V_{bl}$  is the boundary layer velocity at the mid-height of the offset,  
548 and  $\beta$  is the gap width to offset height ratio.

549 In Figure 9 the uplift pressures are presented in a different dimensionless manner, as percentages  
550 of the velocity head computed from the channel-average velocity approaching the simulated  
551 joint. This collapses the data from each study into a single curve for all tested gap widths and

552 offset heights. In Figure 10 the data sets are combined and a single curve fit equation is obtained  
553 with an  $R^2$  value of 0.90:

554 
$$\frac{H_u}{V^2/(2g)} = e^{-0.215-0.679\sqrt{\beta}} \quad (9)$$

555 The variables here are the same as in Eq. 8, except that  $V$  is the average velocity for the full  
556 channel. There is still a tendency at large gap width to offset height ratios for larger uplift  
557 pressures in the open channel data, but at low gap width to offset height ratios the data sets  
558 coincide well. The better curve fit suggests that the actual boundary layer in both experiments  
559 may have been thinner than the calculated estimates, so that the uplift pressures were driven  
560 primarily by the mean-channel velocity. Eq. 9 offers a useful approach to predicting uplift  
561 pressure when there is little or no boundary layer, and is more straightforward to apply than Eq.  
562 8 since it requires determination of only the average channel velocity instead of the more  
563 complex boundary layer velocity profile. Notably, for gap width to offset height ratios less than  
564 0.5 the uplift pressure predicted by Eq. 9 is more than 50% of the channel-average velocity head,  
565 which exceeds the estimates of uplift pressure made by the IFT (2018) for the Oroville Dam  
566 spillway (see Table 1). To apply either Eq. 8 or 9 to a prototype case, the gap width to offset  
567 height ratio must be known, but the uplift pressure is not dependent on the actual offset height or  
568 gap width. In contrast, the IFT (2018) approach used the offset height, but did not consider any  
569 effect of the gap width. Despite these observations, one should not conclude that the magnitude  
570 of the offset height or gap width are unimportant from a practical standpoint, since large  
571 openings to the foundation should enable more flow to get beneath the slab where it can have a  
572 myriad of undesirable affects if not captured and carried away safely. Large openings should  
573 also be expected to enable uplift pressures to extend to larger areas beneath a slab.

## 574 **Scale Effects**

575 One motivation for the water tunnel tests by Frizell (2007) was the possibility of scale effects in  
576 the low-velocity open channel tests of Johnson (1976). Low velocities and Reynolds numbers  
577 might affect turbulence intensity and boundary layer development, which could in turn affect  
578 generated uplift pressures. If Reynolds number effects were present in the laboratory tests, it  
579 should be visible in a comparison of model results obtained at different Reynolds numbers.  
580 Three possible formulations of the Reynolds number could be relevant to this flow situation.  
581 The boundary layer Reynolds number is typically defined as  $Re_x = Vx/\nu$  (Eq. 6), where  $V$  is the  
582 mean velocity in the channel and  $x$  is the length of the boundary layer from the start of its  
583 growth. The two other potentially useful Reynolds numbers are  $Re_w = Vw/\nu$ , where  $w$  is the gap  
584 width, and  $Re_h = Vh/\nu$ , where  $h$  is the offset height.

585 Frizell (2007) was able to test at velocities up to 3 times higher than those used by Johnson  
586 (1976), but the range of gap and offset Reynolds numbers for the two studies was similar, since  
587 Johnson (1976) tested larger gap widths and offsets. To test for Reynolds number effects, the  
588 data for each study were grouped within low, middle, and high ranges of the three Reynolds  
589 numbers and plots like those in Figure 7 and Figure 9 were constructed to see if different ranges  
590 of Reynolds numbers produced different curves. No consistent Reynolds number effects could  
591 be identified that were distinct from the scatter in the data.

## 592 **Application and Research Needs**

593 The Oroville Dam Independent Forensic Team did not use the results of either the Johnson  
594 (1976) or Frizell (2007) studies for prediction of uplift pressures, instead opting to assume that

595 uplift would be equal to the stagnation pressures associated with flow velocity in the boundary  
596 layer at of the mid-height of an offset. The present study reanalyzed the Johnson (1976) and  
597 Frizell (2007) data sets to develop Eq. 8, which relates the uplift pressure to the boundary layer  
598 velocity profile, and Eq. 9 which relates the uplift pressure to the mean velocity in a channel.  
599 Notably, both equations show that there is an important additional effect beyond that assumed by  
600 IFT (2018), namely the influence of the geometric ratio of gap width to offset height. Eq. 9 is  
601 convenient to apply since it does not require estimation of boundary layer velocities. Both  
602 equations are superior to the relations provided by the original studies, since they use  
603 dimensionless forms that do not require matching application details to a specific test run at a  
604 particular velocity, offset height, or gap width. Because Eq. 9 is based on channel-average  
605 velocity rather than boundary layer velocities, it is likely to yield conservatively high estimates  
606 of uplift pressure for long chutes in which boundary layer velocities could be much lower than  
607 average velocities.

608 The uncertainty of Eq. 8 is large, but it still offers potential to be valuable in prototype spillways  
609 with long chutes, since boundary layer effects could reduce uplift pressures significantly.  
610 Through its influence on the boundary layer, spillway surface roughness could be an important  
611 factor, with uniformly rough surfaces having less uplift potential than smooth surfaces. To  
612 further improve this approach to the problem, experimental data are needed from test facilities in  
613 which the boundary layer velocities are significantly different from the channel-average velocity  
614 and can be adjusted and measured. The studies by Johnson (1976) and Frizell (2007) both varied  
615 the average flow velocity significantly, but boundary layer velocities were not measured, and  
616 estimated boundary layer velocities at the mid-height of the tested offsets were typically about  
617 70-90% of the average velocity. For comparison, for the Oroville Dam spillway the estimated

618 boundary layer velocities underlying the stagnation pressure estimates in Table 1 ranged from  
619 about 50-70% of the average velocity.

620 Aerated flow is another factor that could have an important influence, both for its effect on the  
621 boundary layer and for its effect on pressure propagation through joints and resonance within  
622 joints. Aeration effects should be studied after non-aerated conditions are well understood.

623 This study has considered only the uplift pressures generated beneath a slab when the foundation  
624 is sealed. In real spillways, the natural or engineered means for conveying water out of the  
625 foundation and dissipating uplift pressure are also important for determining total uplift forces.  
626 To assess the removal of water from the foundation, it is necessary to estimate amounts of water  
627 entering through spillway joints or cracks. For this purpose, IFT (2018) used equations that  
628 predicted leakage rates due to piezometric pressure heads in the chute (i.e., pressure due only to  
629 the depth of flow); these equations did not reflect any increased flow that might occur due to an  
630 offset projecting into the flow. Currently there is not a good source of laboratory testing to  
631 support making estimates of flow through joints with offsets. Research should be initially  
632 focused on prediction of flow rates assuming fully vented conditions beneath the slab or partially  
633 vented conditions with measurement of the backpressure beneath the slab. For application in the  
634 field, the flow rates estimated for the fully vented condition could be modified based on a  
635 separate analysis of the underlying drainage layer or drainage system.

636 A potentially valuable avenue for further research on this topic is field-scale studies. To the best  
637 of the authors' knowledge, there have been no attempts to measure uplift pressures beneath the  
638 lining of prototype spillways. An instrumented prototype spillway could enable the collection of  
639 data for high-velocity flows with realistic boundary layer and aerated flow conditions.

640 This review was initiated with the goal of developing a research plan to address the influence of  
641 factors such as complex flow paths through spillway joints (effects of keyways, waterstops,  
642 reinforcement, etc.), variations in the openness of joints, and differences in joint configuration  
643 (vertical offsets, spalls, and joints oriented acutely to the flow). However, the review has shown  
644 that there are still fundamental issues that need to be resolved before these complexities are  
645 considered. Until the necessary research can be completed, defensive design practices and  
646 proactive maintenance programs to prevent the widespread existence of open or offset joints are  
647 crucial to defend against hydraulic jacking.

## 648 **Acknowledgments**

649 The authors appreciate the detailed comments of the three anonymous reviewers and the editor  
650 and associate editor. Their constructive criticism led to significant improvement of the paper.

651 The data from the Johnson (1976) study were digitized from the original figures and can be  
652 obtained by e-mail request from the lead author, along with the complete data set from the Frizell  
653 (2007) study. The authors wish to especially acknowledge the work of the late Perry Johnson  
654 who inspired us all and continues to do so today.

655 This work was jointly funded by Reclamation's Science & Technology Program and Dam Safety  
656 Technology Development Program.

## 657 **Notation**

658  $H_u$  = uplift pressure head

659  $\Delta P$  = Pressure difference between chamber below slab and water tunnel flow above slab

660  $P_s$  = stagnation pressure

661  $Q_{joint}$  = flow rate through spillway joint  
662  $Q_{spillway}$  = flow over slab downstream from offset joint  
663  $Q_{total}$  = total flow approaching offset in water tunnel test facility  
664  $Re_x$  = boundary layer Reynolds number based on mean velocity and distance from start of  
665 boundary layer growth,  $Re_x = Vx/\nu$   
666  $Re_w$  = Reynolds number based on mean velocity and gap width,  $Re_w = Vw/\nu$   
667  $Re_h$  = Reynolds number based on mean velocity and offset height,  $Re_h = Vh/\nu$   
668  $V$  = mean flow velocity approaching a spillway joint  
669  $V_{bl}$  = boundary layer velocity at mid-height of an offset  
670  $e$  = base of natural logarithms, 2.7183  
671  $f$  = Darcy-Weisbach friction factor  
672  $g$  = acceleration due to gravity  
673  $h$  = offset height  
674  $u_*$  = shear velocity  
675  $v_y$  = velocity at distance  $y$  above the boundary, approach velocity of the stagnated flow  
676  $w$  = gap width  
677  $x$  = distance from start of boundary layer growth  
678  $y$  = distance from the boundary  
679  $y_0$  = total flow depth  
680  $\beta$  = ratio of gap width to offset height  
681  $\gamma$  = unit weight of water  
682  $\delta$  = boundary layer thickness  
683  $\rho$  = fluid density  
684  $\tau_0$  = bed shear stress  
685  $\nu$  = kinematic viscosity

686

## References

687 Barjastehmaleki, S., V. Fiorotto, and E. Caroni, 2016a. Spillway stilling basins lining design via  
688 Taylor hypothesis. *Journal of Hydraulic Engineering*, 142(6).

689 Barjastehmaleki, S., V. Fiorotto, and E. Caroni, 2016b. Design of stilling basin linings with  
690 sealed and unsealed joints. *Journal of Hydraulic Engineering*, 142(12).

691 Bellin, A. and V. Fiorotto 1995. Direct dynamic force measurement on slabs in spillway stilling  
692 basins. *Journal of Hydraulic Engineering*, 121(10):686-693.

693 [https://doi.org/10.1061/\(ASCE\)0733-9429\(1995\)121:10\(686\)](https://doi.org/10.1061/(ASCE)0733-9429(1995)121:10(686))

694 Bollaert, E. and A. Schleiss, 2003a. Scour of rock due to the impact of plunging high velocity  
695 jets, Part I: A state-of-the-art review, *Journal of Hydraulic Research*, 41(5):451-464,

696 DOI: [10.1080/00221680309499992](https://doi.org/10.1080/00221680309499992)

697 Bollaert, E. and A. Schleiss, 2003b. Scour of rock due to the impact of plunging high velocity  
698 jets, Part II: Experimental results of dynamic pressures at pool bottoms and in one- and

699 two-dimensional closed end rock joints, *Journal of Hydraulic Research*, 41(5):465-480,

700 DOI: [10.1080/00221680309499992](https://doi.org/10.1080/00221680309499992)

701 Bollaert, E., and A. Schleiss, 2005. Physically based model for evaluation of rock scour due to  
702 high-velocity jet impact. *Journal of Hydraulic Engineering*, 131(3):153-165.

703 [https://doi.org/10.1061/\(ASCE\)0733-9429\(2005\)131:3\(153\)](https://doi.org/10.1061/(ASCE)0733-9429(2005)131:3(153))

704 Bowers, C.E. and J. Toso, 1988. Karnafuli Project, model studies of spillway damage. *Journal*  
705 *of Hydraulic Engineering*, 114(5). [https://doi.org/10.1061/\(ASCE\)0733-](https://doi.org/10.1061/(ASCE)0733-9429(1988)114:5(469))  
706 [9429\(1988\)114:5\(469\)](https://doi.org/10.1061/(ASCE)0733-9429(1988)114:5(469))

707 Bureau of Reclamation, 2014. Design Standards No. 14, Appurtenant Structures for Dams  
708 (Spillways and Outlet Works), Chapter 3: General Spillway Design Considerations,  
709 Section 3.8.6. [https://www.usbr.gov/tsc/techreferences/designstandards-](https://www.usbr.gov/tsc/techreferences/designstandards-datacollectionguides/finalds-pdfs/DS14-3.pdf)  
710 [datacollectionguides/finalds-pdfs/DS14-3.pdf](https://www.usbr.gov/tsc/techreferences/designstandards-datacollectionguides/finalds-pdfs/DS14-3.pdf)

711 Dong, Z., Wu, Y., and Zhang, D., 2010. Cavitation characteristics of offset-into-flow and effect  
712 of aeration, *Journal of Hydraulic Research*, 48(1):74-80,  
713 DOI:10.1080/00221680903566083

714 Falvey, H.T. 1990. *Cavitation in Chutes and Spillways*, Engineering Monograph 42, U.S. Dept.  
715 of the Interior, Bureau of Reclamation, Denver, CO.

716 Fiorotto, V. and A. Rinaldo 1992a. Fluctuating uplift and lining design in spillway stilling  
717 basins. *Journal of Hydraulic Engineering*, 118(4). [https://doi.org/10.1061/\(ASCE\)0733-](https://doi.org/10.1061/(ASCE)0733-9429(1992)118:4(578))  
718 [9429\(1992\)118:4\(578\)](https://doi.org/10.1061/(ASCE)0733-9429(1992)118:4(578))

719 Fiorotto, V. and A. Rinaldo, 1992b. Turbulent pressure fluctuations under hydraulic jumps.  
720 *Journal of Hydraulic Research*, 30(4):499-520.  
721 <https://doi.org/10.1080/00221689209498897>

722 Fiorotto, V. and P. Salandin, 2000. Design of anchored slabs in stilling basins. *Journal of*  
723 *Hydraulic Engineering*, 126(7):502-512. [https://doi.org/10.1061/\(ASCE\)0733-](https://doi.org/10.1061/(ASCE)0733-9429(2000)126:7(502))  
724 [9429\(2000\)126:7\(502\)](https://doi.org/10.1061/(ASCE)0733-9429(2000)126:7(502))

725 Fiorotto, V. and E. Caroni, 2014. Unsteady seepage applied to lining design in stilling basins.  
726 *Journal of Hydraulic Engineering*, 140(7).

727 Frizell, K.W., 2007. *Uplift and Crack Flow Resulting from High Velocity Discharges over Open*  
728 *Offset Joints*. Report DSO-07-07, Bureau of Reclamation Dam Safety Technology  
729 Development Program, Denver, CO.  
730 [https://www.usbr.gov/tsc/techreferences/hydraulics\\_lab/pubs/DSO/DSO-07-07.pdf](https://www.usbr.gov/tsc/techreferences/hydraulics_lab/pubs/DSO/DSO-07-07.pdf)

731 González-Betancourt, M. and L. Posada-García, 2016. Effects of joints and their waterstops on  
732 pressures spread over a slab. *DYNA* 83(197):94-103.  
733 <http://dx.doi.org/10.15446/dyna.v83n197.47579>

734 Hepler, T.E., and P.L. Johnson, 1988. Analysis of spillway failures by uplift pressure. In:  
735 *Hydraulic Engineering*, Proceedings of the 1988 National Conference on Hydraulic  
736 Engineering and International Symposium on Model-Prototype Correlations, ASCE,  
737 Colorado Springs, Colorado, Aug. 8-12, 1988. S.R. Abt and J. Gessler, editors.  
738 <http://cedb.asce.org/CEDBsearch/record.jsp?dockkey=0057459>

739 IFT, 2018. *Independent Forensic Team Report: Oroville Dam Spillway Incident*, January 5,  
740 2018. [https://damsafety.org/sites/default/files/files/Independent Forensic Team Report](https://damsafety.org/sites/default/files/files/Independent%20Forensic%20Team%20Report%20Final%2001-05-18.pdf)  
741 [Final 01-05-18.pdf](https://damsafety.org/sites/default/files/files/Independent%20Forensic%20Team%20Report%20Final%2001-05-18.pdf)

742 Johnson, P.L., 1976. Research into uplift on steep chute lateral linings. Memorandum to the  
743 Open and Closed Conduit Systems Committee, Bureau of Reclamation, Denver CO.  
744 [https://www.usbr.gov/tsc/techreferences/hydraulics\\_lab/pubs/PAP/PAP-1163.pdf](https://www.usbr.gov/tsc/techreferences/hydraulics_lab/pubs/PAP/PAP-1163.pdf)

745 Liu, P.Q., and A.H. Li, 2007. Model discussion of pressure fluctuations propagation within  
746 lining slab joints in stilling basins. *Journal of Hydraulic Engineering*, 133(6):618-624.  
747 [https://doi.org/10.1061/\(ASCE\)0733-9429\(2007\)133:6\(618\)](https://doi.org/10.1061/(ASCE)0733-9429(2007)133:6(618))

748 Mahzari, M., and A.J. Schleiss, 2010. Dynamic analysis of anchored concrete linings of plunge  
749 pools loaded by high velocity jet impacts issuing from dam spillways. *Dam Engineering*,  
750 20(4):307-327.

751 Melo, J.F., A.N. Pinheiro, and C.M. Ramos, 2006. Forces on plunge pool slabs: influence of  
752 joints location and width. *Journal of Hydraulic Engineering*, 132(1):49-60.  
753 [https://doi.org/10.1061/\(ASCE\)0733-9429\(2006\)132:1\(49\)](https://doi.org/10.1061/(ASCE)0733-9429(2006)132:1(49))

754 Pells, S., 2016. Erosion of rock in spillways. Doctoral thesis, University of New South Wales,  
755 School of Civil and Environmental Engineering.  
756 [https://www.unsworks.unsw.edu.au/primo-](https://www.unsworks.unsw.edu.au/primo-explore/fulldisplay?docid=unsworks_39826&context=L&vid=UNSWORKS&lang=en_US)  
757 [explore/fulldisplay?docid=unsworks\\_39826&context=L&vid=UNSWORKS&lang=en U](https://www.unsworks.unsw.edu.au/primo-explore/fulldisplay?docid=unsworks_39826&context=L&vid=UNSWORKS&lang=en_US)  
758 [S](https://www.unsworks.unsw.edu.au/primo-explore/fulldisplay?docid=unsworks_39826&context=L&vid=UNSWORKS&lang=en_US)

759 Roberson, J.A., and C.T. Crowe, 1985. *Engineering Fluid Mechanics*, 3<sup>rd</sup> ed., Houghton Mifflin  
760 Company, Boston, MA.

761 Rouse, H., 1945. *Elementary Mechanics of Fluids*. John Wiley & Sons, p. 199.

762 Toso, J.W., and C.E. Bowers, 1988. Extreme pressures in hydraulic-jump stilling basins.  
763 *Journal of Hydraulic Engineering*, 114(8). [https://doi.org/10.1061/\(ASCE\)0733-](https://doi.org/10.1061/(ASCE)0733-9429(1988)114:8(829))  
764 [9429\(1988\)114:8\(829\)](https://doi.org/10.1061/(ASCE)0733-9429(1988)114:8(829))

765 Trojanowski, J., 2004. Assessing failure potential of spillways on soil foundation. Association  
766 of State Dam Safety Officials Annual Conference, Lexington, KY.

767 Trojanowski, J., 2008. DAM SAFETY: Evaluating Spillway Condition, *Hydro Review*, Vol. 27,  
768 Issue 2, April 2008. [https://www.hydroworld.com/articles/hr/print/volume-27/issue-](https://www.hydroworld.com/articles/hr/print/volume-27/issue-2/technical-articles/dam-safety-evaluating-spillway-condition.html)  
769 [2/technical-articles/dam-safety-evaluating-spillway-condition.html](https://www.hydroworld.com/articles/hr/print/volume-27/issue-2/technical-articles/dam-safety-evaluating-spillway-condition.html)

770 Wahl, T.L, K.W. Frizell, and H.T. Falvey, 2019. *SpillwayPro – Tools for Analysis of Spillway*  
771 *Cavitation and Design of Chute Aerators*, Hydraulic Laboratory Report HL-2019-03,  
772 U.S. Dept. of the Interior, Bureau of Reclamation, Denver, CO.

773 **Tables**

774 **Table 1. — Stagnation pressures at Sta. 1006 m (33+00 ft) of the Oroville Dam spillway, at half of**  
 775 **the offset height for three hypothetical offsets.**

Discharge (m <sup>3</sup> /s)	Flow depth (m)	Average velocity (m/s)	Average velocity head (m)	Darcy- Weisbach friction factor, <i>f</i>	Stagnation pressure head at 50% of offset height (m) (and as % of channel-average velocity head)		
					6-mm offset	12-mm offset	25-mm offset
850	0.60	26.1	34.6	0.0132	11.3 (33%)	14.3 (41%)	17.7 (51%)
1530	0.94	30.0	46.0	0.0121	13.8 (30%)	17.3 (38%)	21.5 (47%)

776 Source: Adapted from IFT (2018, Appendix B, Table 2).

777 Note: Errors in the original table are corrected and pressures are provided in SI units and as percentages of channel-  
 778 average velocity head.

## 779 **Figures**

780 Figure 1. — Spillway damage observed after gates were initially closed at midday, February  
781 7, 2017 (DWR photo; reprinted from IFT 2018, with permission).

782 Figure 2. — Ultimate damage at the Oroville Dam service spillway in May 2017 (DWR  
783 photo; reprinted from IFT 2018, with permission).

784 Figure 3. — Johnson (1976) data on uplift pressures in sealed offset joints, as originally  
785 presented in the form of percentages of the channel-average velocity head versus  
786 offset height. Power curve trend lines for each gap width are for illustration only;  
787 Johnson (1976) drew individual curves by hand through the data points for each gap  
788 width and velocity setting.

789 Figure 4. — Plan view of test facility setup showing pump, piping, flow meter, and test  
790 section. The 2.44-m (8-ft) long approach to the test section consisted of a 0.91-m (3-  
791 ft) long round-to-square transition (191-mm [7.5-inch] diameter to 102-mm [4-inch]  
792 square), followed by 1.52 m (5 ft) of 102-mm (4-inch) square duct. (Adapted from  
793 Frizell 2007)

794 Figure 5. — Test chamber used by Frizell (2007). The upstream round-to-square transition is  
795 not yet attached in this photo. The thickness of the upstream slab is 25.4 mm (1 inch).  
796 (Adapted from Frizell 2007)

797 Figure 6. — Test apparatus and location of pressure taps for uplift pressure measurement  
798 (Adapted from Frizell 2007).

799 Figure 7. — Uplift pressure head as a percentage of boundary layer velocity head related to joint  
800 geometry.

801 Figure 8. — Curve relating uplift pressure head to boundary layer velocity and the gap width to  
802 offset height ratio.

803 Figure 9. — Uplift pressure head as a percentage of mean-channel velocity head, related to joint  
804 geometry.

805 Figure 10. — Curve relating uplift pressure head to channel-mean velocity and the gap width to  
806 offset height ratio.

807

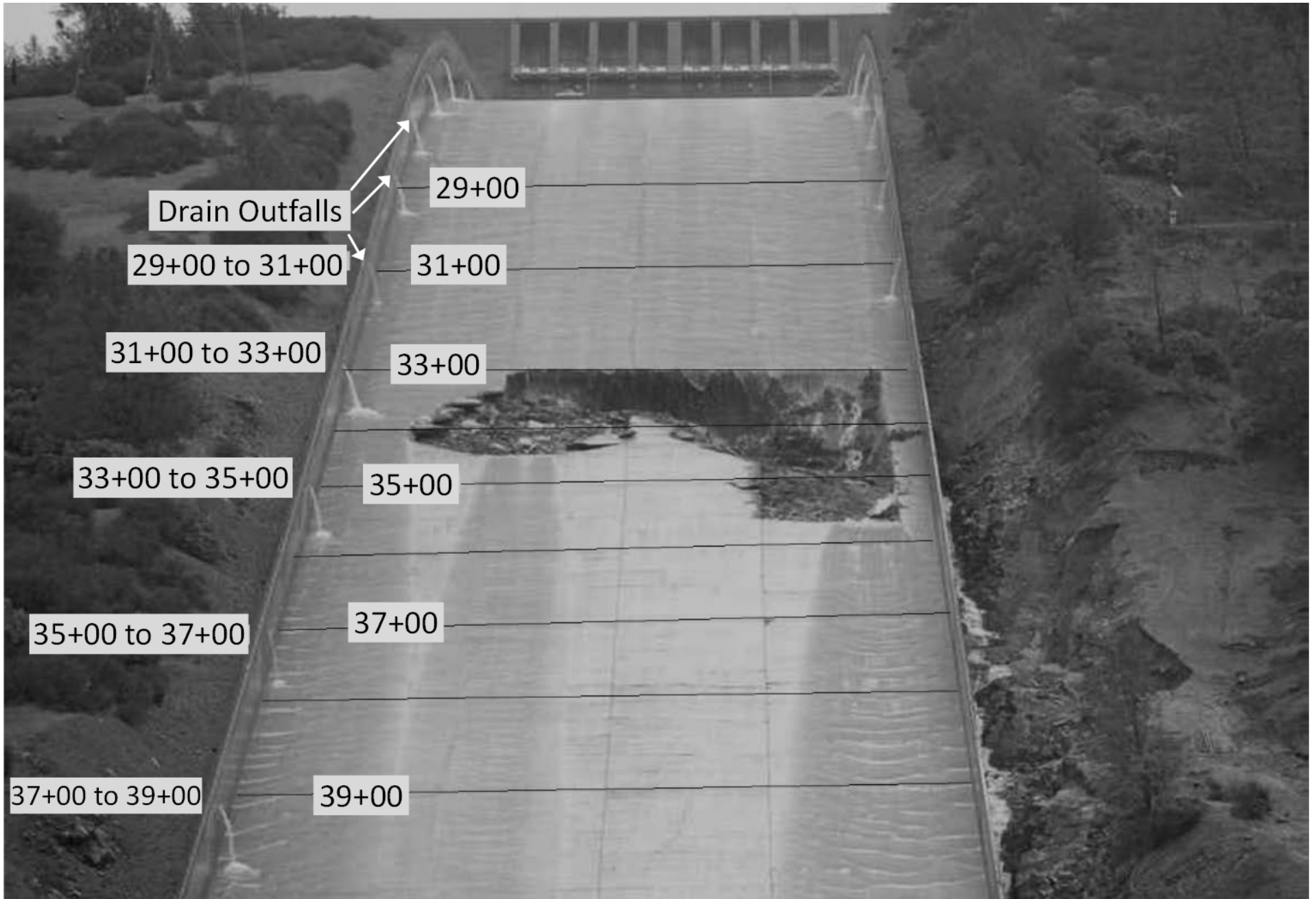


Figure 1. — Spillway damage observed after gates were initially closed at midday, February 7, 2017 (DWR photo; reprinted from IFT 2018, with permission).



Figure 2. — Ultimate damage at the Oroville Dam service spillway in May 2017 (DWR photo; reprinted from IFT 2018, with permission).

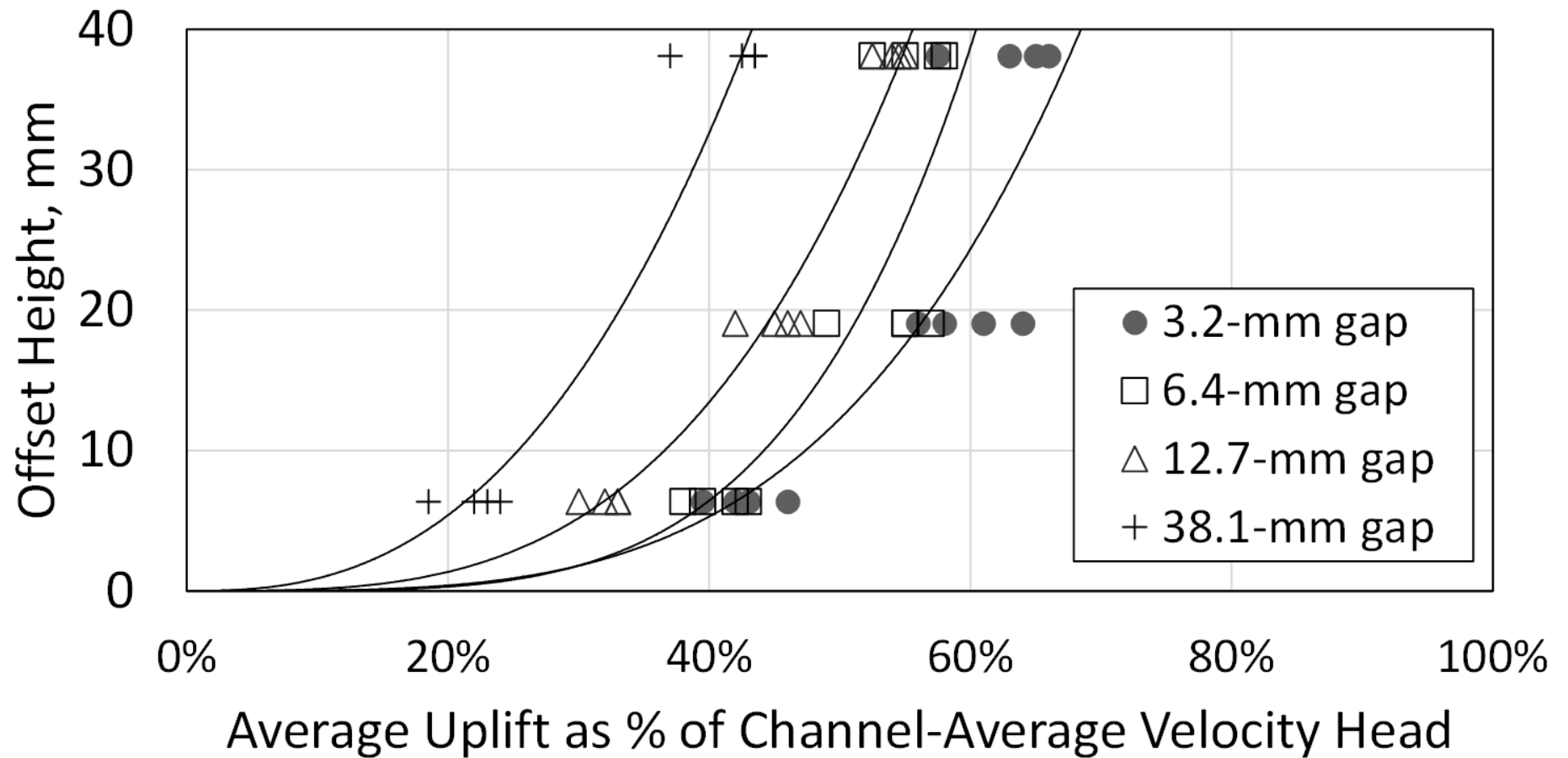


Figure 3. — Johnson (1976) data on uplift pressures in sealed offset joints, as originally presented in the form of percentages of the channel-average velocity head versus offset height. Power curve trend lines for each gap width are for illustration only; Johnson (1976) drew individual curves by hand through the data points for each gap width and velocity setting.

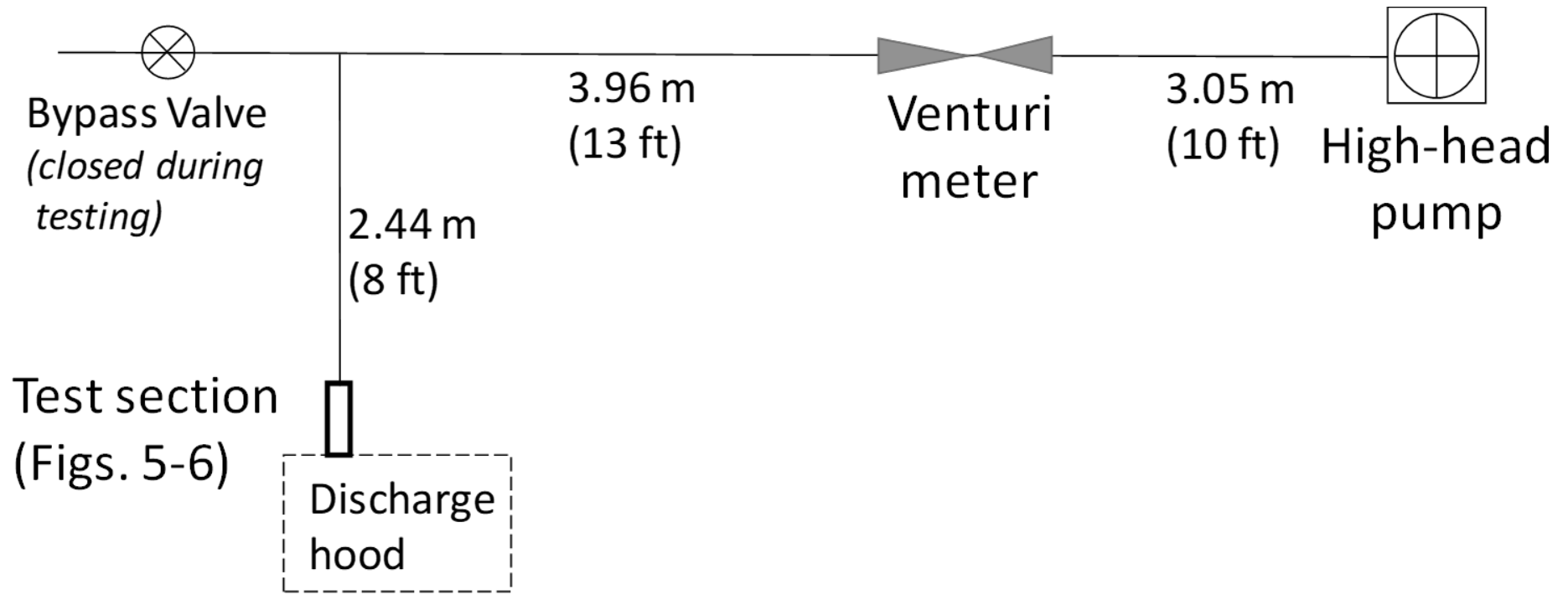


Figure 4. — Plan view of test facility setup showing pump, piping, flow meter, and test section. The 2.44-m (8-ft) long approach to the test section consisted of a 0.91-m (3-ft) long round-to-square transition (191-mm [7.5-inch] diameter to 102-mm [4-inch] square), followed by 1.52 m (5 ft) of 102-mm (4-inch) square duct. (Adapted from Frizell 2007)

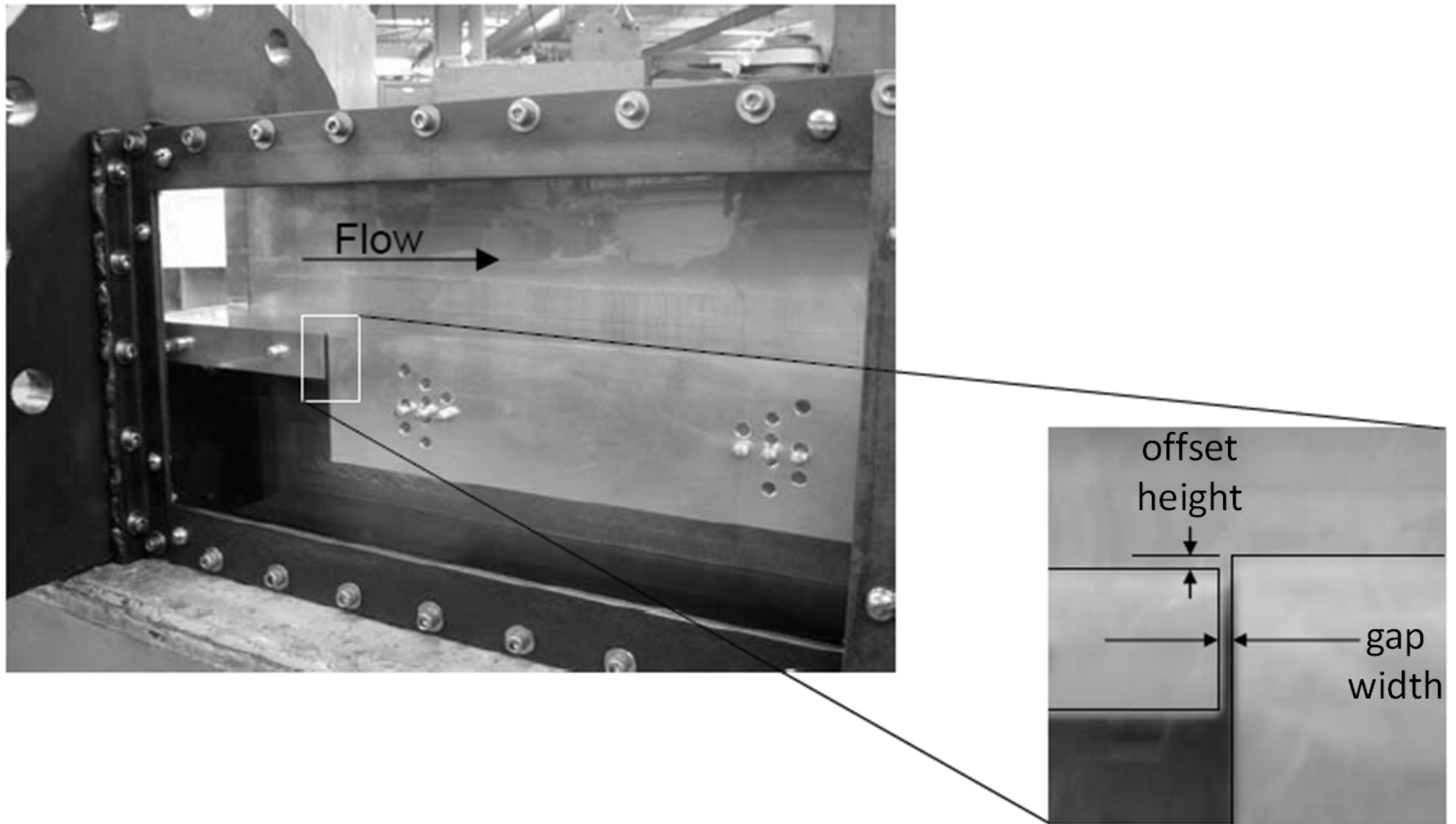
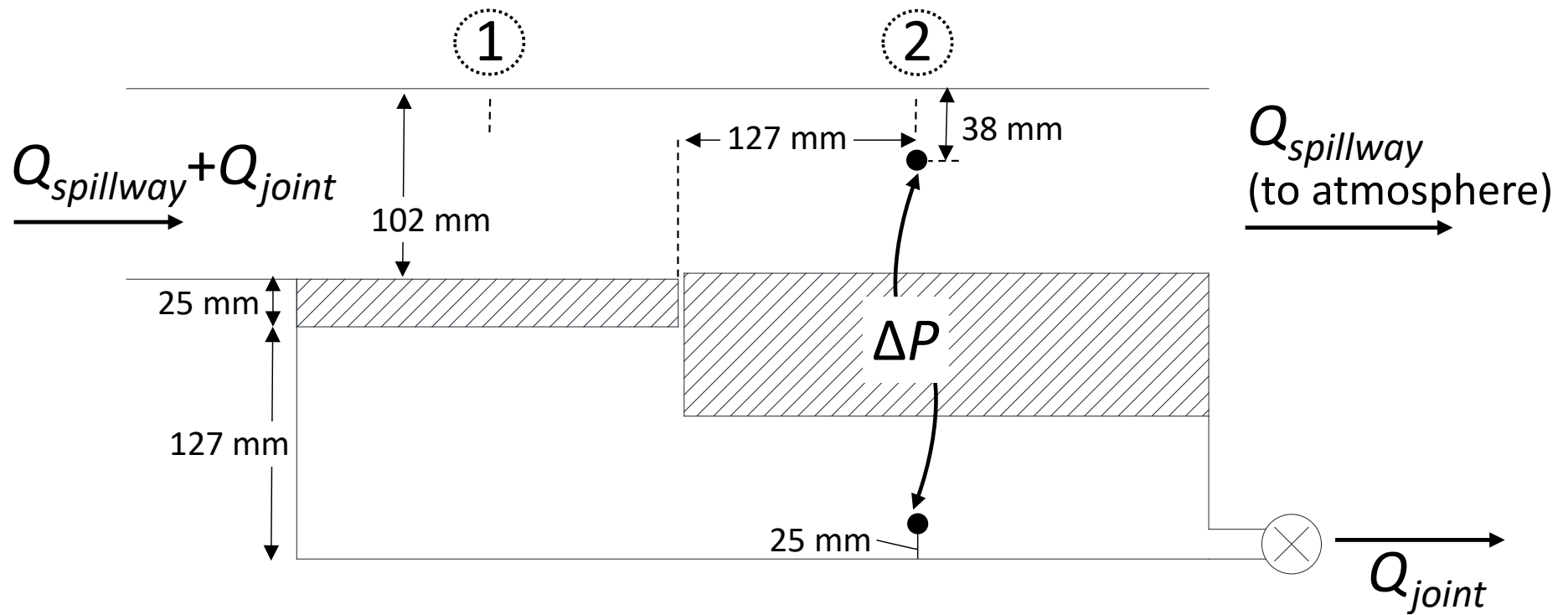


Figure 5. — Test chamber used by Frizell (2007). The upstream round-to-square transition is not yet attached in this photo. The thickness of the upstream slab is 25.4 mm (1 inch). (Adapted from Frizell 2007)



Uplift pressure,  $\Delta P$ , measured by differential transducer across indicated taps

Figure 6. — Test apparatus and location of pressure taps for uplift pressure measurement (Adapted from Frizell 2007).

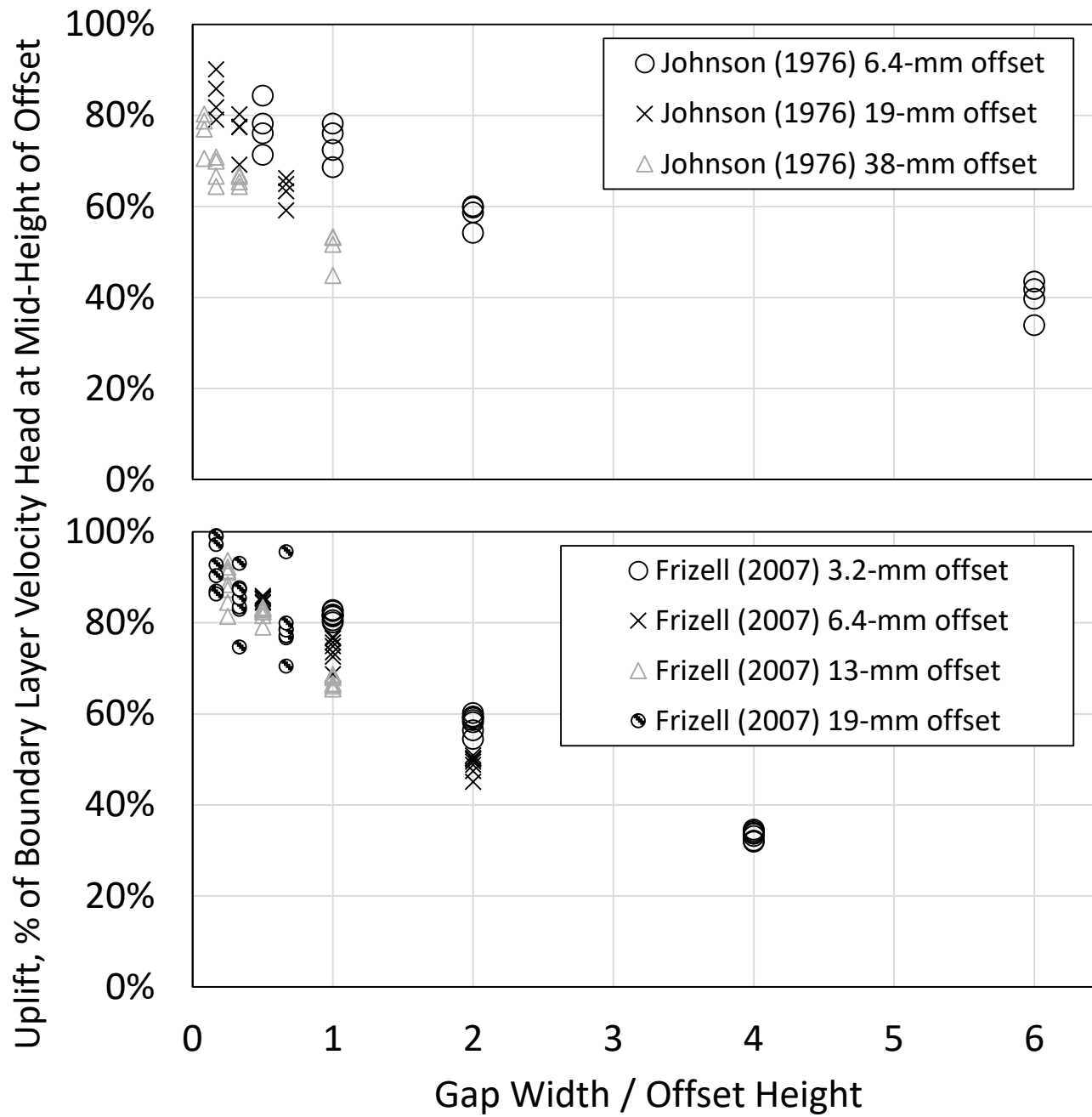


Figure 7. — Uplift pressure head as a percentage of boundary layer velocity head related to joint geometry.

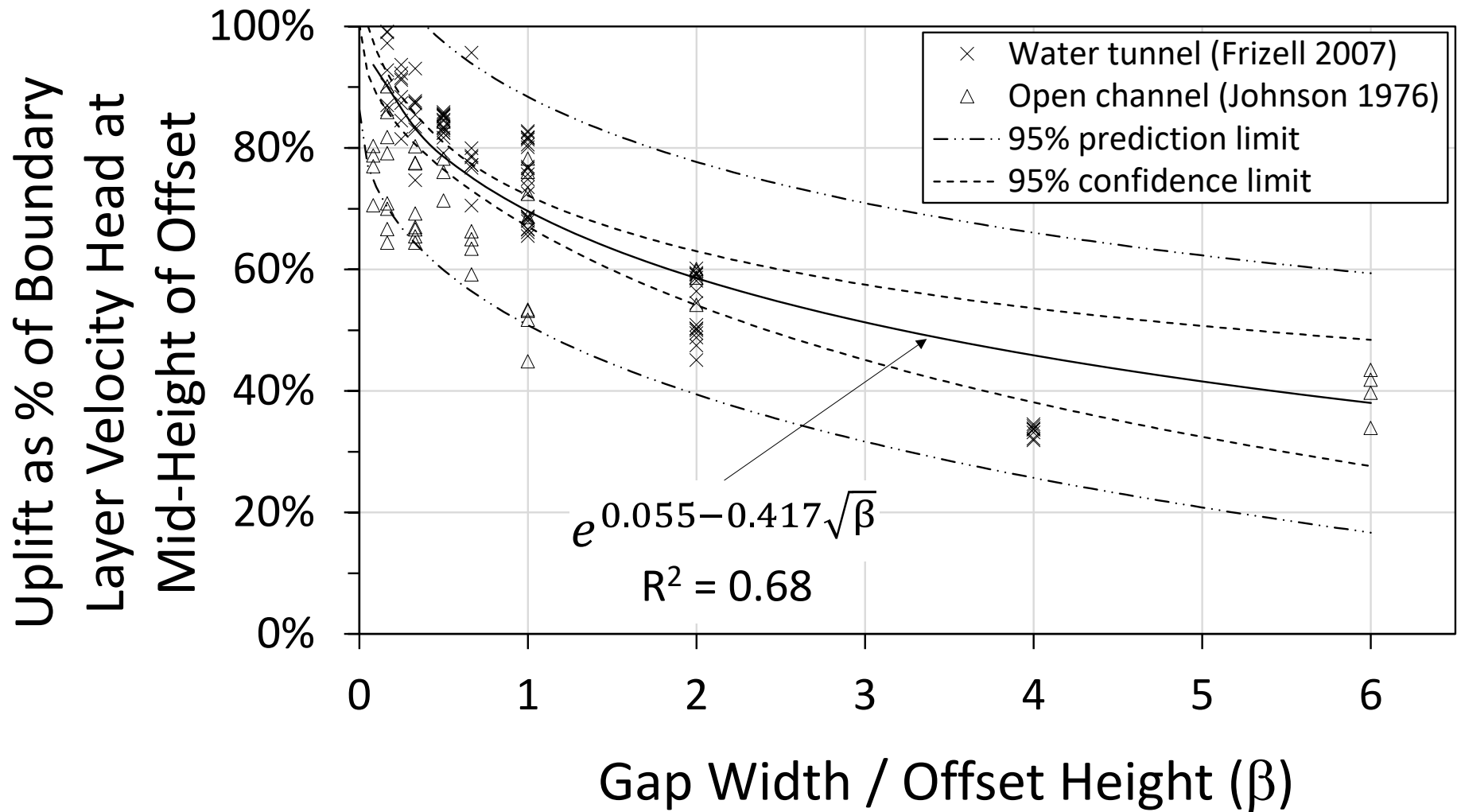


Figure 8. — Curve relating uplift pressure head to boundary layer velocity and the gap width to offset height ratio.

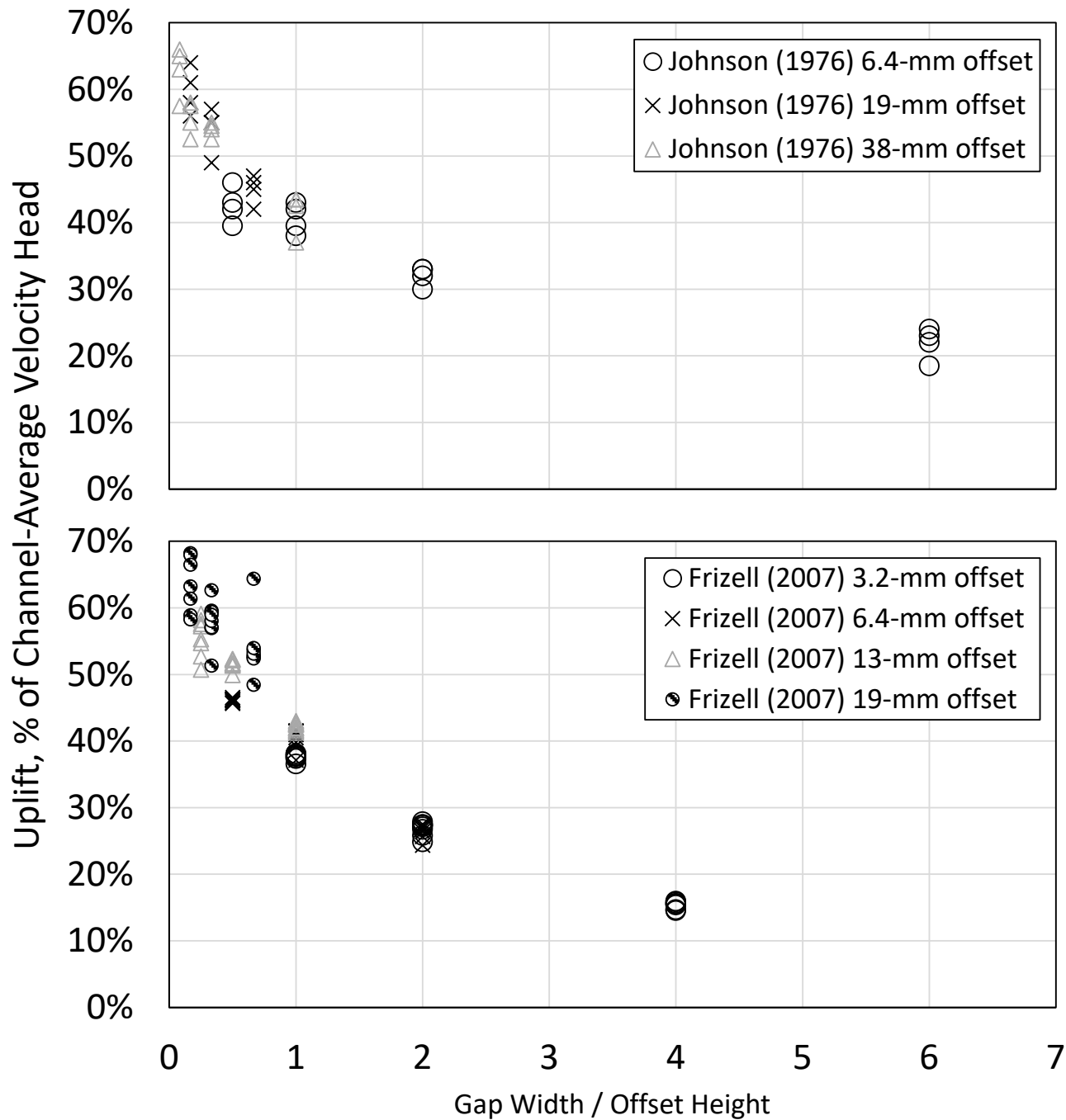


Figure 9. — Uplift pressure head as a percentage of mean-channel velocity head, related to joint geometry.

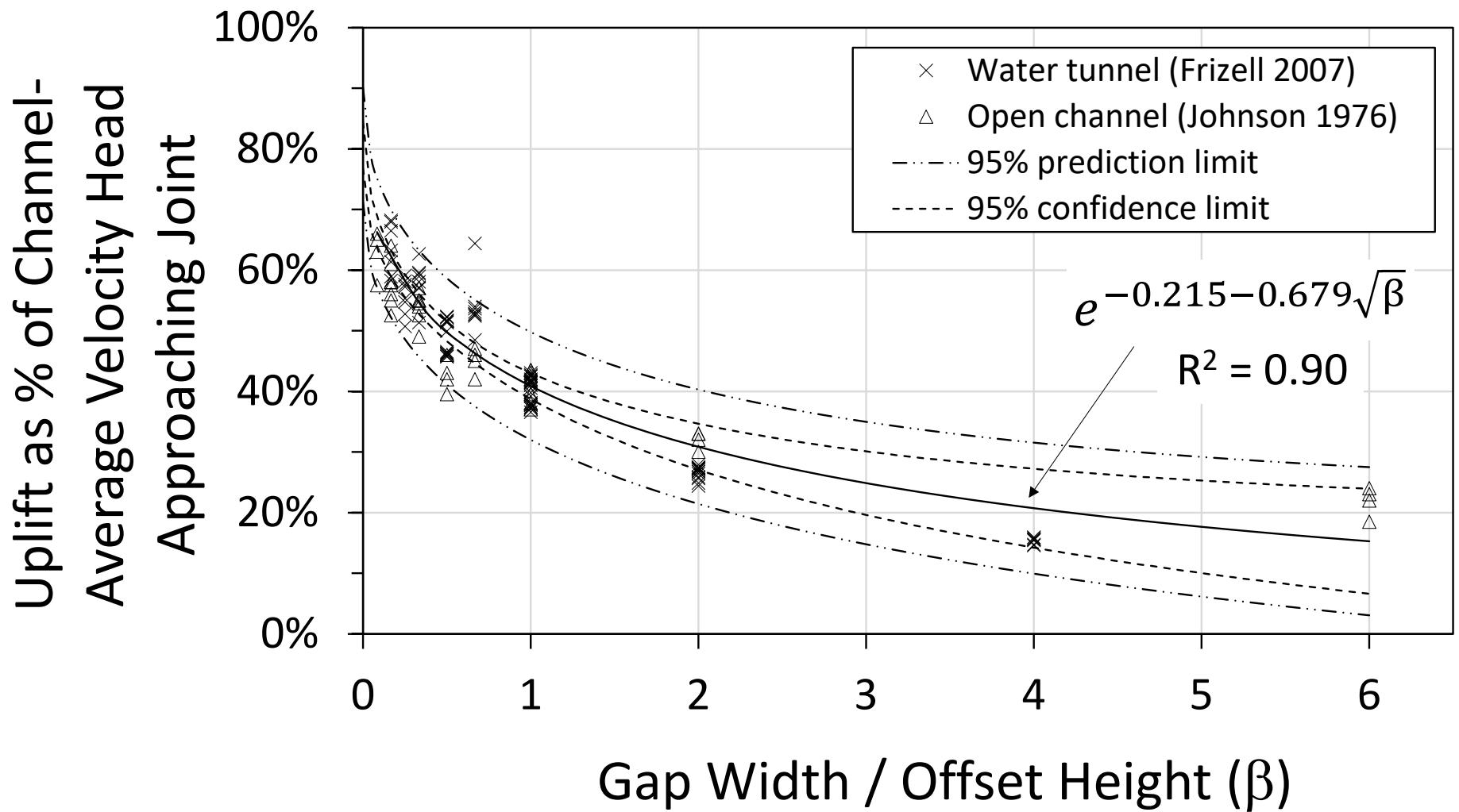


Figure 10. — Curve relating uplift pressure head to channel-mean velocity and the gap width to offset height ratio.